Design advantages and analysis of a novel five-phase doubly-fed induction generator

Roland Ryndzionek, Michal Michna, Filip Kutt, Grzegorz Kostro and Krzysztof Blecharz

Faculty of Electrical and Control Engineering, Gdansk University of Technology, Gdansk, Poland

Received 15 September 2022
Revised 10 February 2023
28 April 2023
Accepted 28 April 2023

Abstract

Purpose – The purpose of this paper is to provide an analysis of the performance of a new five-phase doubly fed induction generator (DFIG).

Design/methodology/approach – This paper presents the results of a research work related to five-phase DFIG framing, including the development of an analytical model, FEM analysis as well as the results of laboratory tests of the prototype. The proposed behavioral level analytical model is based on the winding function approach. The developed DFIG model was used at the design stage to simulate the generator's no-load and load state. Then, the results of the FEM analysis were shown and compared with the results of laboratory tests of selected DFIG operating states.

Findings – The paper provides the results of analytical and FEM simulation and measurement tests of the new five-phase dual-feed induction generator. The use of the MATLAB Simscape modeling language allows for easy and quick implementation of the model. Design assumptions and analytical model-based analysis have been verified using FEM analysis and measurements performed on the prototype. The results of the presented research validate the design process as well as show the five-phase winding design advantage over the three-phase solution regarding the control winding power quality.

Research limitations/implications – The main disadvantage of the winding function approach-based model development is the simplification regarding omitting the tangential airgap flux density component. However, this fault only applies to large airgap machines and is insignificant in induction machines. The results of the DFIG analyses were limited to the basic operating states of the generator, i.e. the no-load state, the inductive and resistive load.

Practical implications – The novel DFIG with five phase rotor control winding can operate as a regular three-phase machine in an electric power generation system and allows for improved control winding power quality of the proposed electrical energy generation system. This increase in power quality is due to the rotor control windings inverter-based PWM supply voltage, which operates with a wider per-phase supply voltage range than a three-phase system. This phenomenon was quantified using control winding current harmonic analysis.

The authors would like to thank the MESCO, an authorized distributor of ANSYS, for granting the Ansys Electronics Desktop license. This work was supported by the Gdańsk University of Technology and IDUB Program under Grant 122020IDUBI.3.3.

COMPEL - The international journal for computation and mathematics in electrical and electronic engineering
Vol. 42 No. 4, 2023
pp. 947-962
Emerald Publishing Limited
0332-1649
DOI 10.1108/COMPEL-09-2022-0333

Originality/value – The paper provides the results of analytical and FEM simulation and measurement tests of the new five-phase dual-feed induction generator.

Keywords Electrical machine, Computer-aided design, Finite element analysis, Time-domain modeling, Electromechanical energy converter, Doubly fed induction generator, Five-phase generator, Analytical modeling, Winding function approach, Finite element model, Winding generator

Paper type Research paper

1. Introduction

The doubly fed induction generators (DFIGs) have well-known advantages of simple constructions and low maintenance and are industrially applicable. They are mainly used in modern wind power plants instead of permanent magnet synchronous generators (Han *et al.*, 2018; Kumar and Choudhary, 2015; Morawiec *et al.*, 2020b; Protsenko and Xu, 2007; Sartaj *et al.*, 2019).

Nowadays, when the industry market increases rapidly, semiconductors and converters are getting cheaper, and different and innovative solutions are being explored. Multiphase machines have several advantages over three-phase systems, such as fault tolerance, higher torque density and lower torque pulsation (Maciejewski and Iwański, 2021; Morawiec *et al.*, 2020a).

This paper presents a behavioral level model of a novel five-phase DFIG based on the winding function approach (WFA). The main advantage of this approach is that the model description is based on actual machine winding distribution and the airgap geometry (Krause *et al.*, 2013; Morawiec *et al.*, 2020a; Szypulski and Iwański, 2018). The main disadvantage of WFA is the simplification regarding omitting the tangential airgap flux density component (Krause *et al.*, 2013; Szypulski and Iwański, 2018). However, this fault only applies to large airgap machines and is insignificant in induction machines (Adamowicz *et al.*, 2015; Kołodziejek and Wachowiak, 2022).

The developed model objective is to verify the modeling approach for further model development. The proposed model based on the WFA should be relatively easy to simplify and convert to the arbitrary orthogonal reference frame. The model should also allow for further development and incorporation of selected physical phenomena such as internal machine asymmetry, nonsinusoidal winding distribution and magnetic saturation of the core. The model developed based on WFA and defined using multiphase machine variables meets said criteria.

This effort aims to present a complete research cycle, including the design and modeling stage, prototype manufacturing and the laboratory test of the novel five-phase DFIG in selected operating conditions. The detailed comparison between three-phase and five-phase DFIGs has been described in Ryndzionek *et al.* (2022). The five-phase DFIG has a significant advantage over existing constructions, an operation with a damaged excitation phase (or even two phases). The aim is that the generator can operate for a longer period without a breakdown, thereby reducing the downtime caused by power electronics failures.

The main contribution of the presented research is to validate the proposed model-based design approach and to verify the improved electrical power quality of the control winding.

The paper is organized as follows: the structure of the developed five-phase DFIG is introduced (Figure 1), and its principle of operation and mathematical model is described in Section 2. The FEM simulation of the prototype is presented in Section 3. Section 4 explains the manufacturing of the prototypes and experimental analysis. Finally, the paper ends with a summary of the obtained results.

2. Mathematical model of five-phase doubly fed induction generator

The specifications of the prototype DFIGs used in this study are shown in Table 1. This generator has a six-pole, three-phase stator winding with one parallel branch and was

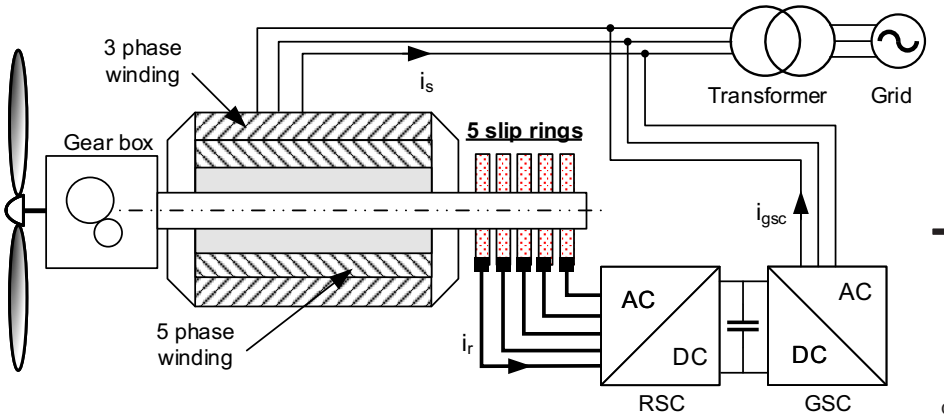

Source: Authors' own work

Figure 1. Scheme of the developed novel five-phase DFIG

Parameter		Value
Rated power	Pn	4 kW
Voltage	Un	400 V
Pair poles	P	3
Stator phases	Ms	3
Rotor phases	Mr	5
Stator slots	Qs	36
Rotor slots	*Qr*	30
Airgap length	Lg	0.3 mm
Axial length	Ls	149
Stator external diameter	Dse	208 mm
Rotor external diameter	Dre	147 mm

Source: Authors' own work

Table 1. Specifications of the prototype DFIG

constructed in a frame size of 132 mm. The generator has been developed using the original stator from a 5.5 kW Sg132m-6 induction motor. The five-phase rotor control winding and core have been designed from scratch to fit and perform with the original core and winding of the selected induction motor.

The rotor was manufactured with a set of five slip rings.

The machine design was based on a predetermined minimum and maximum speed, the set output electric power and the maximum rotor voltage ($U_r < U_s$) corresponding with the operating speed range.

2.1 Basic model of the five-phase doubly fed induction generator

The stator and rotor voltage equations describe the general form of the five-phase DFIG model:

$$\mathbf{U_s} = \mathbf{R_s I_s} + \frac{d}{dt}\mathbf{\Psi_s} \tag{1}$$

$$\mathbf{U_r} = \mathbf{R_r I_r} + \frac{d}{dt}\mathbf{\Psi_r} \tag{2}$$

where:
$\mathbf{U_s}$, $\mathbf{U_r}$ = stator and rotor voltage vectors;
$\mathbf{I_s}$, $\mathbf{I_r}$ = stator and rotor current vectors;
$\mathbf{R_s}$, $\mathbf{R_r}$ = stator and rotor resistance matrix; and
$\mathbf{\Psi_s}$, $\mathbf{\Psi_r}$ = stator and rotor flux linkage vectors.

The flux linkage equation for the stator and rotor winding is:

$$\begin{bmatrix} \mathbf{\Psi_s} \\ \mathbf{\Psi_r} \end{bmatrix} = \begin{bmatrix} \mathbf{L_{ss}} & \mathbf{L_{sr}} \\ \mathbf{L_{sr}^T} & \mathbf{L_{rr}} \end{bmatrix} \begin{bmatrix} \mathbf{I_s} \\ \mathbf{I_r} \end{bmatrix} \tag{3}$$

where:
$\mathbf{L_{ss}}$, $\mathbf{L_{rr}}$ = inductance matrix of stator and rotor windings; and
$\mathbf{L_{sr}}$ = the matrix of mutual inductances between stator and rotor windings.

The five-phase DFIG model completes the mechanical equation:

$$t_{em} = t_l + J\frac{d}{dt}\omega + D\omega \tag{4}$$

where:
t_{em} = electromagnetic torque;
t_l = load torque;
J = a moment of the rotor and load inertia;
ω = rotor speed; and
D = damping factor.

The magnetomotive force of the stator winding:

$$\begin{aligned} MMF_{as}(\varphi_s) &= \frac{N_s}{2} i_{as}(t)\cos(\varphi_s) \\ MMF_{bs}(\varphi_s) &= \frac{N_s}{2} i_{bs}(t)\cos\left(\varphi_s - \frac{2}{3}\pi\right) \\ MMF_{cs}(\varphi_s) &= \frac{N_s}{2} i_{cs}(t)\cos\left(\varphi_s + \frac{2}{3}\pi\right) \end{aligned} \tag{5}$$

where N_s is the number of stator conductors.

The stator winding distribution is represented by:

$$N_{xs} = \frac{1}{i_{ixs}(t)}\frac{d}{dt} MMF_{xs}(\varphi_s) \tag{6}$$

$$\begin{aligned} N_{as}(\varphi_s) &= -\frac{N_s}{2}\sin(\varphi_s) \\ N_{bs}(\varphi_s) &= -\frac{N_s}{2}\sin\left(\varphi_s - \frac{2}{3}\pi\right) \\ N_{cs}(\varphi_s) &= -\frac{N_s}{2}\sin\left(\varphi_s + \frac{2}{3}\pi\right) \end{aligned} \tag{7}$$

The general stator flux density distribution has been represented by:

$$B_{xs}(\varphi_s) = \frac{\mu_0}{\delta} MMF_{xs}(\varphi_s) \tag{8}$$

The detailed stator flux density distribution:

$$\begin{aligned} B_{as}(\varphi_s) &= \frac{N_s}{2}\frac{\mu_0}{g} i_{as}(t)\cos(\varphi_s) \\ B_{bs}(\varphi_s) &= \frac{N_s}{2}\frac{\mu_0}{g} i_{bs}(t)\cos\left(\varphi_s - \frac{2}{3}\pi\right) \\ B_{cs}(\varphi_s) &= \frac{N_s}{2}\frac{\mu_0}{g} i_{cs}(t)\cos\left(\varphi_s + \frac{2}{3}\pi\right) \end{aligned} \tag{9}$$

where i_{as}, i_{bs} and i_{cs} are stator phase current.

Finally, the flux linkage is described by:

$$\Psi_{xs}(\varphi_s) = r \cdot l \cdot \int_{\varphi_s}^{\varphi_s+\pi} B_{xs}(\zeta) d\zeta \tag{10}$$

Thus, the stator flux linkage is:

$$\begin{aligned} \Psi_{as}(\varphi_s) &= -\frac{\mu_0 N_s l r}{g} i_{as}(t)\sin(\varphi_s) \\ \Psi_{bs}(\varphi_s) &= -\frac{\mu_0 N_s l r}{g} i_{bs}(t)\sin\left(\varphi_s - \frac{2}{3}\pi\right) \\ \Psi_{cs}(\varphi_s) &= -\frac{\mu_0 N_s l r}{g} i_{cs}(t)\sin\left(\varphi_s + \frac{2}{3}\pi\right) \end{aligned} \tag{11}$$

The rotor winding distribution:

$$\begin{aligned} N_{ar}(\varphi_r) &= -\frac{N_r}{2}\sin(\varphi_r) \\ N_{br}(\varphi_r) &= -\frac{N_r}{2}\sin\left(\varphi_r - \frac{2}{5}\pi\right) \\ N_{cr}(\varphi_r) &= -\frac{N_r}{2}\sin\left(\varphi_r - \frac{4}{5}\pi\right) \\ N_{dr}(\varphi_r) &= -\frac{N_r}{2}\sin\left(\varphi_r + \frac{4}{5}\pi\right) \\ N_{er}(\varphi_r) &= -\frac{N_r}{2}\sin\left(\varphi_r + \frac{2}{5}\pi\right) \end{aligned} \tag{12}$$

And the rotor flux linkage is:

$$\begin{aligned}
\Psi_{ar}(\varphi_r) &= -\frac{\mu_0 N_r l r}{g} i_{ar}(t)\sin(\varphi_r) \\
\Psi_{br}(\varphi_r) &= -\frac{\mu_0 N_r l r}{g} i_{ar}(t)\sin\left(\varphi_r - \frac{2}{5}\pi\right) \\
\Psi_{cr}(\varphi_r) &= -\frac{\mu_0 N_r l r}{g} i_{cr}(t)\sin\left(\varphi_r - \frac{4}{5}\pi\right) \\
\Psi_{dr}(\varphi_r) &= -\frac{\mu_0 N_r l r}{g} i_{dr}(t)\sin\left(\varphi_r + \frac{4}{5}\pi\right) \\
\Psi_{er}(\varphi_r) &= -\frac{\mu_0 N_r l r}{g} i_{er}(t)\sin\left(\varphi_r + \frac{2}{5}\pi\right)
\end{aligned} \tag{13}$$

Stator self-inductance a is:

$$L_{asas}(\varphi_s) = \frac{1}{i_{as}(t)}\int_{-\frac{\pi}{2}}^{\frac{\pi}{2}} N_{as}(\zeta)\ \Psi_{as}(\zeta)d\zeta = \left(\frac{N_s}{2}\right)^2 \frac{\pi\mu_0 r l}{g} \tag{14}$$

And stator mutual inductances a are also the same:

$$L_{asbs}(\varphi_s) = \frac{1}{i_{bs}(t)}\int_{-\frac{\pi}{2}}^{\frac{\pi}{2}} N_{as}(\zeta)\ \Psi_{bs}(\zeta)d\zeta = \frac{1}{2}\left(\frac{N_s}{2}\right)^2 \frac{\pi\mu_0 r l}{g} = -\frac{1}{2}L_{ms} \tag{15}$$

Self-inductance of ar winding:

$$L_{arar} = \frac{1}{i_{ar}(t)}\int_{-\frac{\pi}{2}}^{\frac{\pi}{2}} N_{ar}(\zeta)\ \Psi_{ar}(\zeta)d\zeta = \left(\frac{N_r}{2}\right)^2 \frac{\pi\mu_0 r l}{g} = L_{ms} \tag{16}$$

Rotor winding mutual inductances concerning the ***ar*** phase:

$$\begin{aligned}
L_{arbr} &= \frac{1}{i_{br}(t)}\int_{-\frac{\pi}{2}}^{\frac{\pi}{2}} N_{ar}(\zeta)\ \Psi_{br}(\zeta)d\zeta = \left(\frac{N_r}{2}\right)^2 \frac{\pi\mu_0 r l}{g}\cos\left(\frac{2}{5}\pi\right) = L_{mr}\cos\left(\frac{2}{5}\pi\right) \\
L_{arcr} &= \frac{1}{i_{cr}(t)}\int_{-\frac{\pi}{2}}^{\frac{\pi}{2}} N_{ar}(\zeta)\ \Psi_{cr}(\zeta)d\zeta \\
L_{ardr} &= \frac{1}{i_{dr}(t)}\int_{-\frac{\pi}{2}}^{\frac{\pi}{2}} N_{ar}(\zeta)\ \Psi_{dr}(\zeta)d\zeta \\
L_{arer} &= \frac{1}{i_{er}(t)}\int_{-\frac{\pi}{2}}^{\frac{\pi}{2}} N_{ar}(\zeta)\ \Psi_{er}(\zeta)d\zeta
\end{aligned} \tag{17}$$

The stator magnetizing inductance is defined as:

$$L_{mr} = \left(\frac{N_r}{2}\right)^2 \frac{\pi \mu_0 r l}{g} \tag{18}$$

The rotor magnetizing inductance is defined as:

$$L_{mr} = \left(\frac{N_r}{2}\right)^2 \frac{\pi \mu_0 r l}{g} \tag{19}$$

where g is the length of the air gap, r is the external radius of the rotor and l is the axial length of the generator.

2.2 Model implementation

The equations of the DFIG mathematical model presented in the previous chapter were used to develop the generator simulation model.

An important issue was selecting an appropriate environment for simulating electromechanical systems. The MATLAB Simscape software was chosen to simulate and analyze selected DFIG operating states. On the one hand, this program has a library with many electromechanical, electrical and electronic components. On the other hand, it offers a physical modeling language for developing custom models.

Simulations in MATLAB Simcape are performed by the idea of physical modeling, in which even a complex system consists of elements (models) representing physical components and their real connections. Using this approach, it is possible to model multidomain systems, where you can integrate components from different physical systems (electrical, mechanical, hydraulic, thermal, etc.).

The DFIG component model was developed as a new component using the Simscape physical modeling language. The model has been defined in a text file whose structure conforms to the language specification. The most important sections of the model include:

- declaration, where the types and names of parameters;
- branches, in which it contains the relation between variables and terminals, between through and across variables; and
- equation, where behavioral model equations are defined.

Selected lines of the developed DFIG component file, representing the main sections of the model, are presented in the following listing.

```
component DFIG % component name
  nodes
  % as stator nodes
  as1 = foundation.electrical.electrical;
  as2 = foundation.electrical.electrical;
  (...)
  end
  variables
  ias = 0, 'A'; % as current
  vas = 0, 'V'; % as voltage
  fas = 0, 'Wb'; % as flux linkage
  ang = 0, 'rad'; % rotor angular position
```

```
(...)
end
parameters
Lsr = 0.29, 'H'; % mutual inductance
Rs = 2.5, 'Ohm'; % stator resistance
(...)
end
branches
ias: as1.i -> as2.i; % stator current
(...)
end
equations
vas == as1.v - as2.v; % stator voltage
(...)
Lasar == Lsr*cos(p*ang); % mutual inductance
(...)
vas == ias*Rs + fas.der; % stator equation
(...)
end
```

The main advantage of this approach is the possibility of intuitive writing of differential equations without the necessity to analyze the specific requirements of numerical methods.

To define a derivative, in the equation section, the operator "der" should be added to the appropriate variable.

The self and mutual inductances of the generator windings are defined according to the equations presented in Section 2 and can be easily modified to take into account higher harmonics.

The developed DFIG model was used to simulate the generator's no-load and load state.

The generator is driven at a constant speed, and the rotor control windings are supplied with alternating currents shifted in phase by $2/5\pi$. The generator load level is controlled by changing the value of the resistance connected to the stator terminals. The amplitude and frequency of the rotor currents and rotor speed are adjusted to the measurement conditions. The parameters of the DFIG model are calculated based on the design data, the no-load test and the short-circuit test (Table 2).

In the no-load state (Figure 2), the flux in the machine is excited by the flow of rotor currents. The no-load voltage amplitude ($U_s 0_m$) induced in stator winding is defined by:

Parameter	
Stator resistance, $\mathbf{R_s}$	2.5 Ω
Rotor resistance, $\mathbf{R_r}$	2.2 Ω
Stator-rotor mutual inductance, $\mathbf{L_{sr}}$	0.29 H
Stator winding leakage inductance, $\mathbf{L_{ls}}$	15 mH
Rotor winding leakage inductance, $\mathbf{L_{lr}}$	15 mH
Motor damping constant, $\mathbf{B_m}$	5.3×10^{-3} m^2 kg/s
Rotor inertia, $\mathbf{J_w}$	0.028 kg
Number of pair poles, **p**	3
Stator to rotor turn ratio, $\mathbf{N_s/N_r}$	2.2

Source: Authors' own work

ble 2.
e-phase DFIG
del parameters

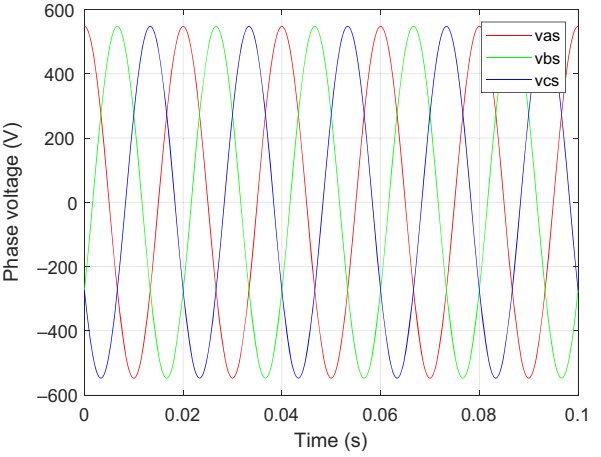

Source: Authors' own work

Figure 2.
No-load voltage waveforms – simulation results

$$U_{s0m} = \frac{5}{2} L_{sr} I_{rm} (\omega_r + p\omega_{rm}) \tag{20}$$

where:

L_{sr} = amplitude of the mutual inductance between stator and rotor windings;
I_{rm} = amplitude of rotor current;
fr = frequency of rotor current; and
ω_{rm} = angular velocity of the rotor.

Two components can be distinguished in the induced voltage of the stator. Transformation-induced voltage is related to the frequency of rotor current changes and rotation-induced voltage resulting from the rotation of the excitation field.

Moreover, the load simulation has been developed. The result of the simulation has been presented in Figure 3.

Finally, the analytical calculation from the model has been compared with the measurement results (Figure 4). The model shows very high convergence, and the other measurement results will be presented in Section 4.

3. The FEA analysis of five-phase doubly fed induction generator

The five-phase DFIG has been designed using the 3D CAD software also. The simulations were conducted to verify the analytical design calculated dimensions and parameters. The Ansys Maxwell and RMxprt design have been used. Moreover, FEA validated the designed prototype's capability to perform in different operating conditions.

The complete model is used to build the model, and its total number of mesh elements is roughly 12,000. The results are almost the same as the model with 20,000 elements. The time step in the transient simulation was 0.2 ms, and the recorded field distribution was at 2 ms. During the FEM analysis, the rotor control winding was excited by five-phase voltage source using an external circuit model. The simulations have been performed for the generator operation in off-grid conditions with a resistive load connected to the stator terminals. Both the on-load and no-load tests have been conducted.

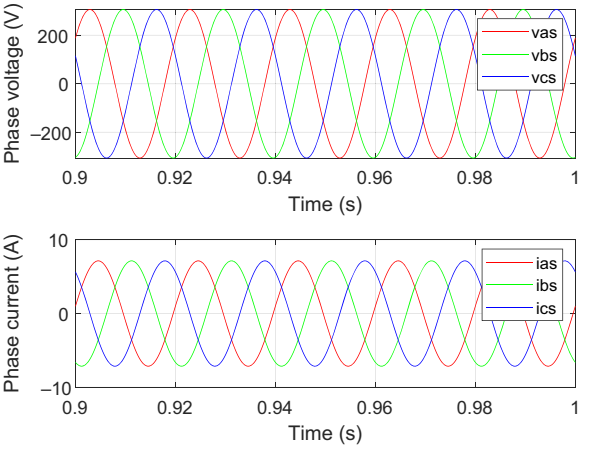

Figure 3.
Voltage and current waveforms under resistive load – simulation results

Source: Authors' own work

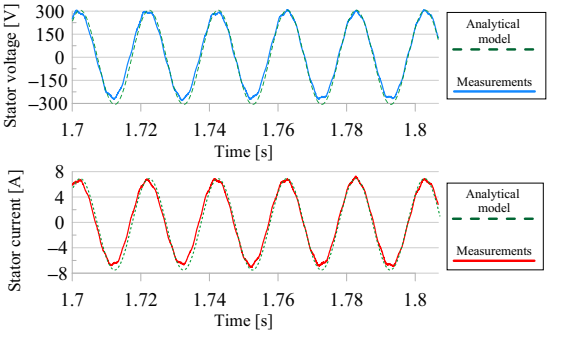

Figure 4.
Experimental and analytical calculation results under the resistive load

Source: Authors' own work

Figure 5 shows the 2D and 3D FEM simulations of DFIG's flux density distribution. The maximum value of flux density is 1.4 T, and the results of both simulations are similar. However, the 3D simulations better represent the phenomenon of slot harmonics.

The maximum value of flux density in the air gap is 0.75 T (Figure 6). The results fit in desired ranges. Moreover, the flux distribution corresponds to the stator and rotor slots distribution.

The simulation results will be compared in Section 4.

4. Laboratory tests

This paper uses measurements to analyze and validate the performance benefits of the proposed five-phase DFIG and verify the developed prototype construction (Figure 7). The primary purpose of the laboratory test was to verify the five-phase DFIG operation at different electric load and rotational velocity conditions.

The measurement was performed at a constant speed of 810 rpm without any load. The DFIG stator is star-connected, and the measurements have been made for different rotor currents.

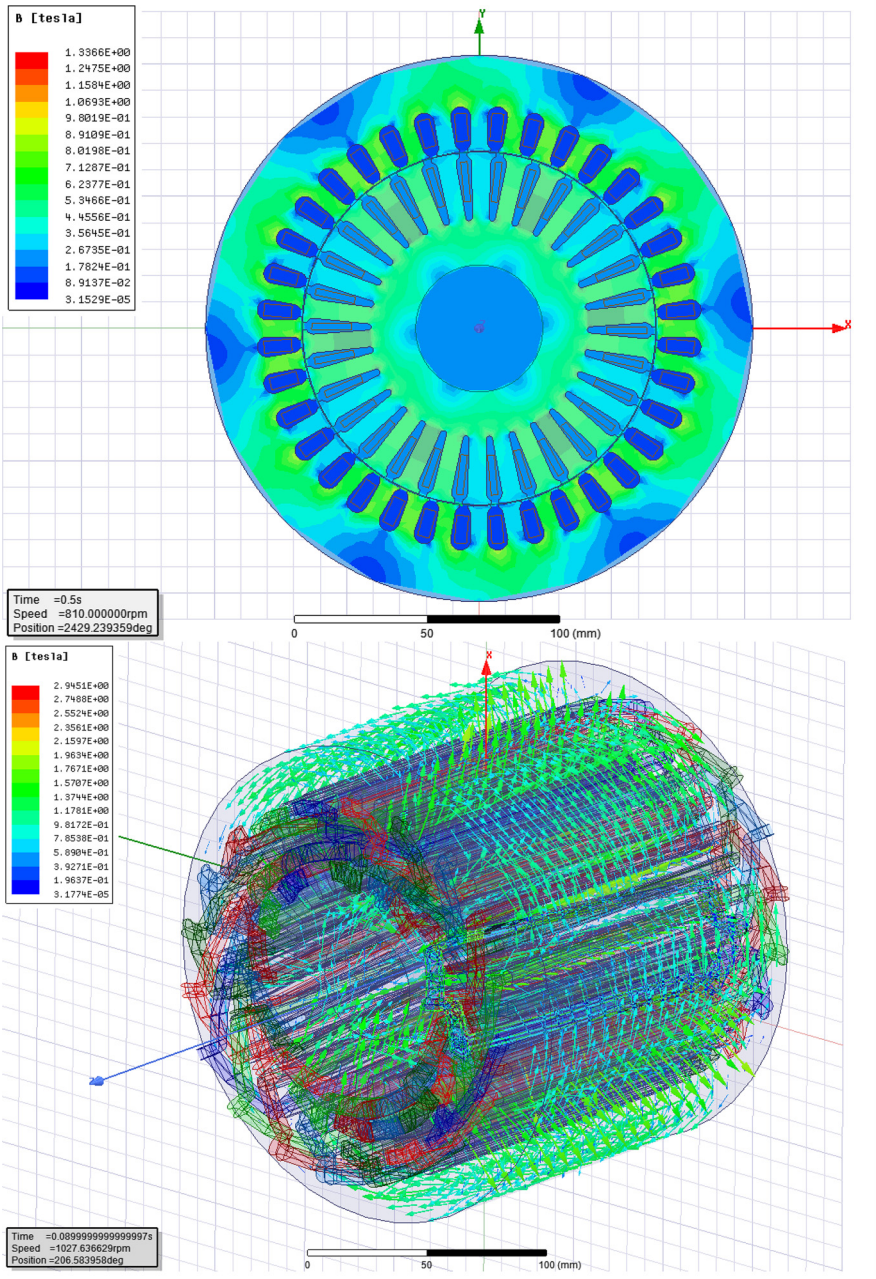

Source: Authors' own work

Figure 5.
FEA 2D and 3D simulation of the stator and rotor core flux density distribution

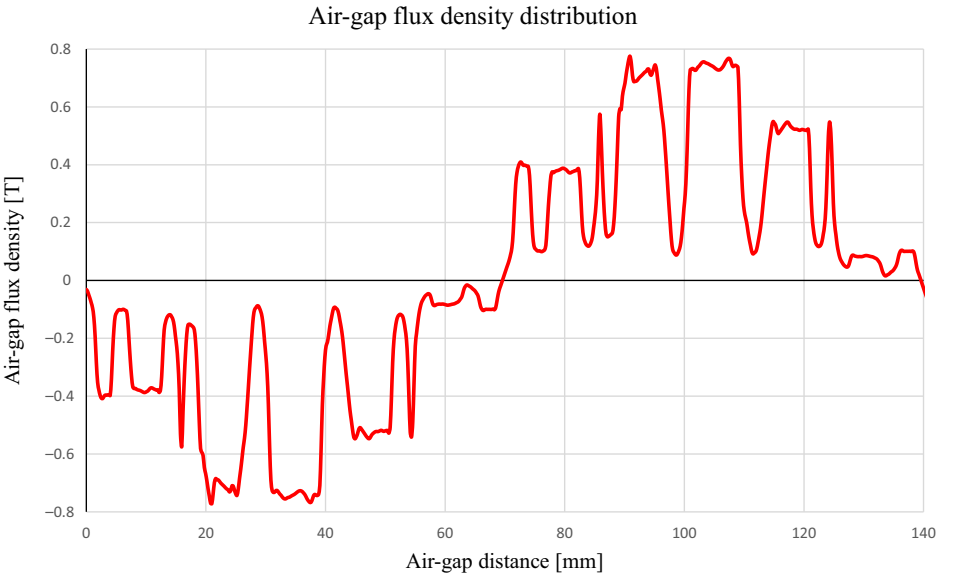

Figure 6.
Air gap magnetic flux distribution using FEA software

Source: Authors' own work

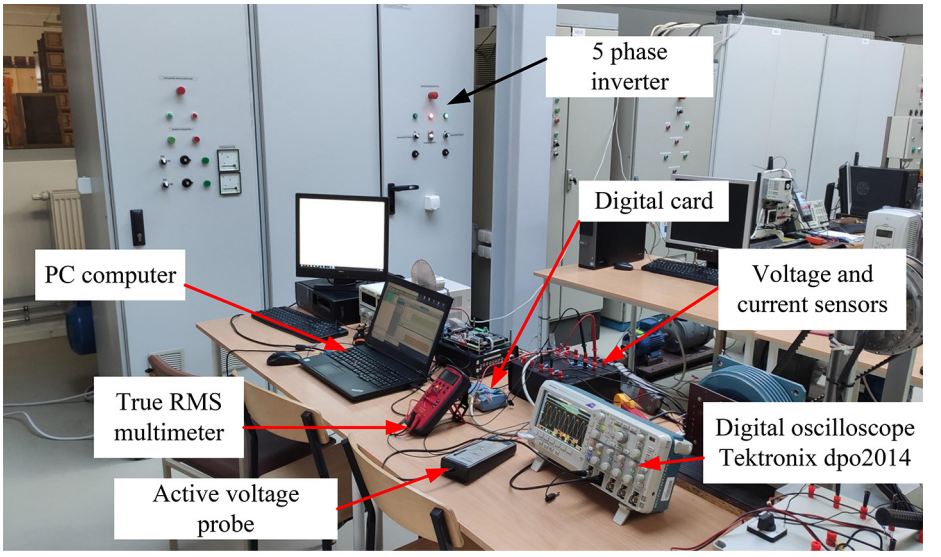

ure 7.
t bench of the
el five-phase
G

Source: Authors' own work

Those measurements have been compared with simulation results.

Figure 8 shows experimental test results. The rotor current exciting the machine is raised several times over the measurement period. These results have been compared with the FEA simulations (with the third and fourth/final steps in the rotor current rising sequence).

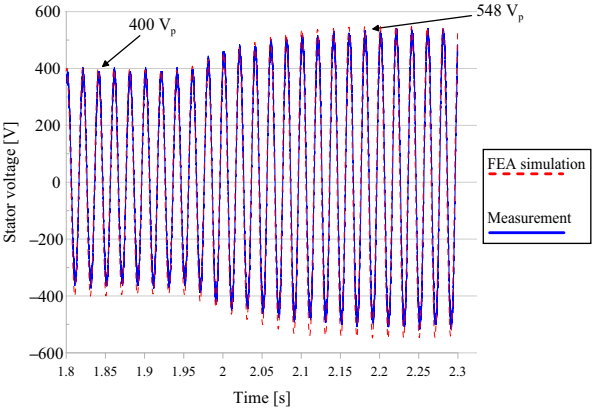

Source: Authors' own work

Figure 8. Induced voltage measurement and simulation under the rotor current exciter (I_r RMS = 1.0 A and 1.5 A)

Moreover, the open circuit characteristics of the rotor currents (Figure 9) and stator voltage (Figure 10) have been presented.

The measurements and FEA simulation results are shown in Figures 11 and 12. The waveforms show good convergence between simulations and measurements, around 10–15 V. The second measurement has been performed with different load conditions (resistive and inductive). In Figure 12, the mixed load has been performed. The active and reactive power was approximately 2 kW and 0.5 kVar.

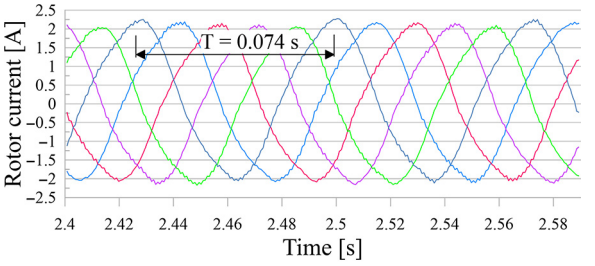

Source: Authors' own work

Figure 9. Five-phase rotor current waveforms (I_r RMS = 1.5 A)

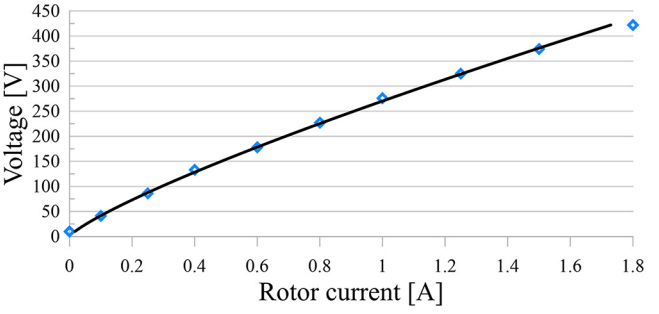

Source: Authors' own work

Figure 10. Open-circuit characteristic (induced voltage vs rotor current)

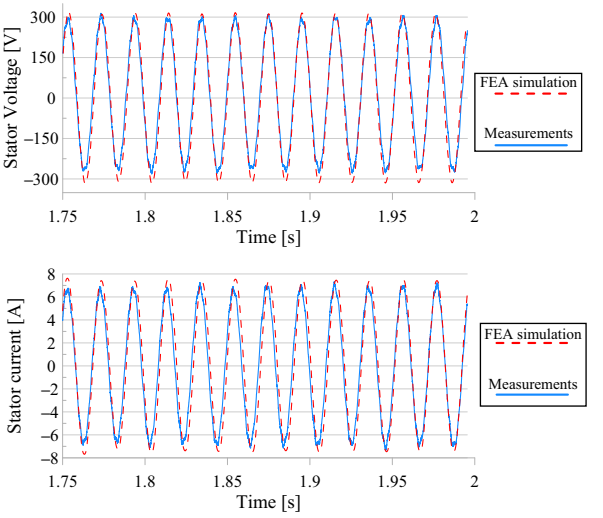

Source: Authors' own work

Figure 11.
Experimental and FEA simulation results under the resistive load

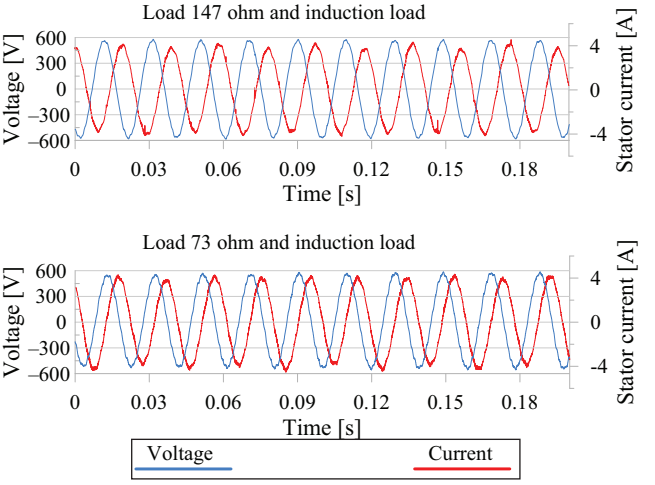

Source: Authors' own work

Figure 12.
Experimental test under the resistive and inductive load

One of the main design advantages of the multiphase control winding is more flexible frequency converter control, where more advanced PWM control strategies can be implemented (Szczepankowski *et al.*, 2021). The main advantage is the improvement in the rotor control winding supply current quality. Figures 13 and 14 show the control winding supply current in three- and five-phase rotor winding and the amplitude spectrum of those currents. The overall THD coefficient for the five-phase control winding is lower than for the three-phase one, demonstrating the higher quality of the supply rotor current.

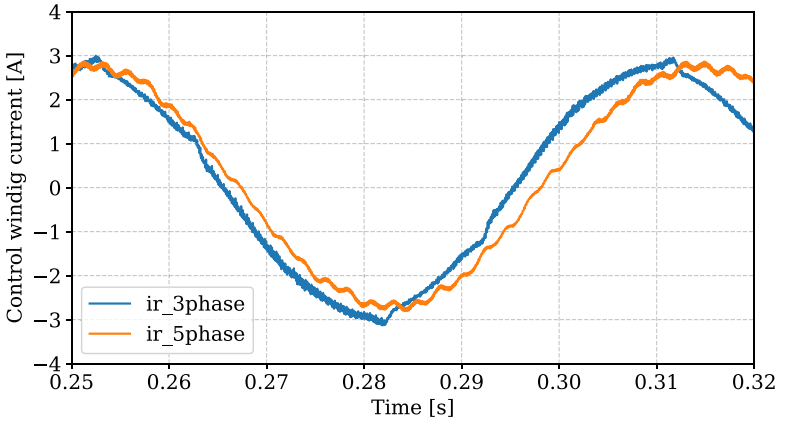

Source: Authors' own work

Figure 13.
Rotor control winding current waveform

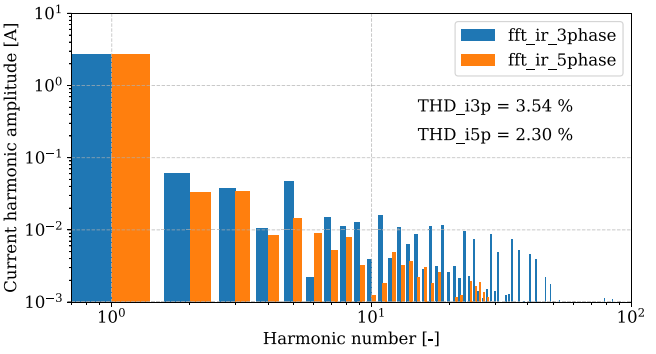

Source: Authors' own work

Figure 14.
Rotor control winding current amplitude spectrum and THD values

5. Conclusions

This paper proposes a novel five-phase DFIG dedicated to modern wind power plants. The proposed generator has been developed, and a prototype machine has been manufactured and tested under different operating conditions. Design assumptions and analytical model-based calculations have been verified using FEM analysis and measurements performed on the prototype. The DFIG with five-phase rotor can operate as a regular three-phase machine in an electric power generation system. Further investigation into the machine's performance will focus on coping with output power quality during single or even dual rotor phase control winding failures due to the inverter or the slip ring assembly fault. However, even with the standard motor stator, the machine could supply the load with both active and reactive power.

References

Adamowicz, M., Guzinski, J. and Krzeminski, Z. (2015), "Nonlinear control of five phase induction motor with synchronized third harmonic flux injection", *2015 First Workshop on Smart Grid and Renewable Energy (SGRE)*, pp. 1-6.

Han, P., Cheng, M., Wei, X. and Jiang, Y. (2018), "Steady-state characteristics of the dual-stator brushless doubly fed induction generator", *IEEE Transactions on Industrial Electronics*, Institute of Electrical and Electronics Engineers Inc., Vol. 65 No. 1, pp. 200-210.

Kołodziejek, P. and Wachowiak, D. (2022), "Fast real-time RDFT- and GDFT-based direct fault diagnosis of induction motor drive", *Energies*, Vol. 15 No. 3, p. 1244.

Krause, P., Wasynczuk, O., Sudhoff, S. and Pekarek, S. (2013), "Analysis of electric machinery and drive systems", *Analysis of Electric Machinery and Drive Systems*, John Wiley and Sons, Inc., doi: 10.1002/9781118524336.

Kumar, P. and Choudhary, R. (2015), "Study of doubly fed induction generator characteristics", *International Journal of Recent Research Aspects*, Vol. 2, pp. 1-6.

Maciejewski, P. and Iwański, G. (2021), "Six-phase doubly fed induction machine-based standalone DC voltage generator", Bulletin of the Polish Academy of Sciences: Technical Sciences.

Morawiec, M., Blecharz, K. and Lewicki, A. (2020a), "Sensorless rotor position estimation of doubly fed induction generator based on backstepping technique", *IEEE Transactions on Industrial Electronics*, Institute of Electrical and Electronics Engineers Inc., Vol. 67 No. 7, pp. 5889-5899.

Morawiec, M., Strankowski, P., Lewicki, A., Guzinski, J. and Wilczynski, F. (2020b), "Feedback control of multiphase induction machines with backstepping technique", *IEEE Transactions on Industrial Electronics*, Institute of Electrical and Electronics Engineers Inc., Vol. 67 No. 6, pp. 4305-4314.

Protsenko, K. and Xu, D. (2007), "Modeling and control of brushless doubly-fed induction generators in wind energy applications", *APEC 07 – Twenty-Second Annual IEEE Applied Power Electronics Conference and Exposition*, IEEE, doi:10.1109/APEX.2007.357565.

Ryndzionek, R., Blecharz, K., Kutt, F., Michna, M. and Kostro, G. (2022), "Fault-tolerant performance of the novel five-phase doubly-fed induction generator", *IEEE Access*, Vol. 10, pp. 59350-59358, doi: 10.1109/ACCESS.2022.3179815.

Sartaj, M., Khan, M.R. and Khan, M.F. (2019), "Modelling of five-phase induction generator incorporating magnetic cross saturation effect", *Proceedings – 2019 International Conference on Electrical, Electronics and Computer Engineering*, UPCON 2019, Institute of Electrical and Electronics Engineers Inc., doi:10.1109/UPCON47278.2019.8980177.

Szczepankowski, P., Strzelecka, N. and Romero-Cadaval, E. (2021), "A new approach to the PWM modulation for the multiphase matrix converters supplying loads with open-end winding", *Energies*, Vol. 14 No. 2, p. 466, doi: 10.3390/en14020466.

Szypulski, M. and Iwański, G. (2018), "Synchronization of state-feedback-controlled doubly fed induction generator with the grid", *Bulletin of The Polish Academy of Sciences Technical Sciences*, Vol. 66 No. 5, doi: 10.24425/bpas.2018.125334.

Corresponding author
Michal Michna can be contacted at: michal.michna@pg.edu.pl